First-principles study of phase stability of bcc XZn (X = Cu, Ag, and Au) alloys

O. Alsalmi,[1] M. Sanati,[1,2] R. C. Albers,[2] T. Lookman,[2] and A. Saxena[2]
[1]*Physics Department, Texas Tech University, Lubbock, Texas 79409-1051, USA*
[2]*Theoretical Division, Los Alamos National Laboratory, Los Alamos, New Mexico 89404, USA*

(Received 22 May 2018; published 5 November 2018)

First-principles density-functional theory is used to study the phase stability/instability and anomalies in the formation of the high-temperature bcc phases of XZn (X = Cu, Ag, and Au) alloys. Although from perhaps a naive point of view, their properties are expected to monotonically depend on the noble-metal (X) column position in the periodic table, this is not the case. For example, the middle-column AgZn alloy has a lower bcc order-disorder (critical) temperature than the CuZn and AuZn alloys above and below in the column. It is shown that this and other nonmonotonic behaviors can be explained in terms of a competition between atomic-size effects and X-atom d-orbital spatial extent. For example, charge-density studies and pair-potential modeling of XZn alloys show that the effective Ag-Zn bond is significantly weaker than either the Cu-Zn or Au-Zn bond at their respective equilibrium lattice constants. We find that an increased atomic-core size effect initially weakens the X-Zn bonding as one goes from CuZn to AgZn, but then the larger d-orbital spatial extent for higher principal quantum numbers becomes a more dominant effect and increases the bonding from AgZn to AuZn. This study is focused on the highly symmetric cubic high-temperature phases, where relative bond-strength magnitudes should be far more important than any bond-directionality effects; the lattice parameters, bulk moduli, elastic constants, Debye temperatures, heats of formation, and order-disorder temperatures for the bcc phases of the three XZn alloys are calculated and compared with experiment.

DOI: 10.1103/PhysRevMaterials.2.113601

I. INTRODUCTION

The properties of CuZn (brass) alloys such as resistance to corrosion, excellent ductility, cold working, machinability, and relative ease of production give them wide applicability [1]. AgZn alloys, when used as battery cell materials, have low internal resistance, high energy density, low weight, and very reliable operation in different (harsh) environments [2,3], and have therefore been long used in military, aerospace, and medical industries. AuZn alloys have been the subject of experimental and theoretical studies [4,5] due to their shape memory effect and the nature of their phase transformation. Because of their wide range of usage and application, the phase diagram of alloys constituted from the noble metals Cu, Ag, and Au and the divalent metal Zn have been the subject of investigations that include the nature of the phases under cooling and/or pressure, and studies of their electronic structures and physical properties [4,6–24].

We characterize these three materials as XZn alloys, where X = Cu, Ag, and Au, respectively a $3d$, $4d$, and $5d$ noble metal from the same column of the periodic table. Since the periodic table is supposed to organize and order various properties, one might naively expect the XZn phase diagrams and properties to be monotonic as one goes down the column. But they are not. In this paper we explore the reason why they are not, which allows a deeper understanding into the interrelationship between the electronic structure and bonding and other material properties of all three of these important materials, in a way that could not be achieved by looking at each material individually.

Near the equiatomic concentration at high temperatures the majority of these materials form in body-centered cubic (β) phases that are disordered, except for AuZn. After lowering the temperature or quenching from high temperatures, most of the disordered alloys in the β phase are retained at room temperature as a metastable ordered body-centered cubic (β_1) phase. Upon further cooling and cold working, the β_1 phases usually transform structurally through a martensitic transformation into new phases. For example, the CuZn alloy transforms from a bcc disordered phase ($A2$) into the CsCl ordered ($B2$) structure. After further cooling, the $B2$ phase transforms martensitically to an orthorhombic structure [6–9]. The AuZn alloy also transforms martensitically to an orthorhombic structure known as the R phase, but retains its ordered $B2$ phase all the way up to its melting point [10,22].

Slow cooling of the disordered $A2$ AgZn alloy causes a structural phase transformation at 540 K. This structure is a complex hexagonal structure (η phase) closely related to the bcc structure, but with nine atoms per unit cell in partially ordered arrangements [11–14]. However, when quenched to room temperature the $A2$ phase changes to a metastable $B2$ phase. No structural phase transformation has been observed with further cooling of the $B2$ phase. Furthermore, by heating the $B2$ phase to about 440 K it transforms to an η phase [14].

It might be expected that an isoelectronic system, where X = Cu, Ag, and Au belong to the same column of the periodic table, would all have similar electronic properties. This is confirmed for the densities of states and d bond energy calculated in this work (Sec. VII). However, cohesive energy and related properties should be different. By moving down the periodic table column and changing the d orbital from $3d$ (Cu) to $4d$ (Ag) to $5d$ (Au), the main electronic effect is a more extended d orbital. The atomic wave function of each

higher principal quantum number needs an additional node in order to be orthogonal to the wave functions of lower principal quantum number. This makes the wave functions bend more to include this node, increasing the curvature (and hence the ∇^2 or Laplacian operator). This increase in the kinetic energy of the orbital can increasingly compensate for the attractive electromagnetic force of the positive nucleus making the wave function of the orbitals extend farther away from the nucleus. As this occurs, the bonding between the X and Zn atoms is expected to become monotonically stronger for a fixed X-Zn interatomic distance, since the X-atom d orbitals hybridize more strongly with the Zn orbitals. Therefore, the bcc phase (ordered and disordered) of XZn systems might be assumed to follow the same trend with AuZn being the most stable (lowest formation energy) phase and CuZn the least stable.

However, the phase diagram of these alloys does not show such a trend. Instead, the critical temperatures for the order-disorder transition of the $B2$ phase in CuZn, AgZn, and AuZn are significantly different. Estimated values for XZn (X = Cu, Ag, and Au) alloys are 763, 518, and 1240 K, respectively [6,10]. Also, only the CuZn system has stable ordered and disordered bcc structures. By comparison, the disordered bcc phase of AgZn is stable at high temperatures while the $B2$ phase is metastable. In the case of the AuZn alloys, the site disorder seems to be absent and the ordered bcc ($B2$) phase extends all the way up to the melting temperature.

More generally, if the underlying physical properties only depended on a single variable like the spatial extent of the noble-metal d orbital, the properties might be expected to be monotonic. To explain properties that have either a maximum or a minimum as a function of the principal quantum number of the noble element that alloys with Zn, as is seen in much of the data (see below), requires a competition between two different underlying causes that push the property in opposite directions. In the present case, we will show that this competition is between (1) effects caused by the increasing size of the atomic cores of the noble metals, and (2) the spatial extent of the noble-metal d orbitals. With increasing principal quantum number, the larger atomic cores push the noble-metal atoms farther away from the Zn atoms reducing the effective hybridization (and hence the bonding) between the noble-metal d orbitals and the Zn orbitals, and counteracting the effect of the greater spatial extent of the d orbitals with higher principal quantum number that causes increased hybridization and bonding. Only the type of quantitative calculations that we perform here can determine which effect is stronger or more dominant at smaller or larger principal quantum number.

To study this, we used first-principles methods to investigate the formation energies of the ordered and disordered bcc phases of XZn (X = Cu, Ag, and Au) alloys, which can provide a quantitative measure of the effective X-Zn hybridization overlaps (bond strengths). The stability of each structure was carefully studied by analyzing their chemical and elastic formation energies; a fit of the band-structure calculations to a Morse pair-potential model [25] allowed us to make a direct comparison of the relative X-Zn bonding strengths. In addition, the charge-density distribution and partial density of states were also examined in detail to improve our understanding of the nature of the X-Zn interactions. We find that the increased atomic-size effect initially weakens the X-Zn bonding as one goes from CuZn to AgZn, but then the larger d-orbital size effect overcomes this and increases the bonding as one goes from AgZn to AuZn.

This paper is organized as follows: Section II describes the details of calculations. Section III discusses the atomic-size effects by calculating the chemical and elastic formation energies. In Sec. IV the pair-potential modeling and its results are discussed. Section V contains the charge and partial density of states analysis. Section VI contains the results of stability of $B2$ versus $A2$ structures at finite temperature. A summary of our results is presented in the last section.

II. DETAILS OF CALCULATIONS

In the present work we use the first-principles density-functional package VASP [26–28] with the generalized-gradient approximation (GGA) to the exchange-correlation potential, and the parameters recommended by Perdew, Burke, and Ernzerhof [29]. The VASP code is a projector augmented-wave technique; our plane-wave cutoff kinetic energy is 400 eV [30,31]. The solution of the generalized self-consistent Kohn-Sham equation employs efficient matrix-diagonalization routines based on the sequential band-by-band residual minimization technique and a Pulay-like charge-density mixing [32]. The pseudopotentials of Cu, Ag, Au, and Zn were provided by the VASP package.

In this calculation, the electronic degrees of freedom were optimized with a conjugate-gradient algorithm, and the lattice constants and ionic atomic positions of the unit cell were totally relaxed. A two-atom periodic cell was used for most of the calculations. The k-point integration in the Brillouin zone was done via a modified tetrahedron method ($24 \times 24 \times 24$ mesh) [33].

The elastic constants were calculated by monitoring relative changes in the total energy as the lattice was strained. For a symmetric cubic structure there are three independent elastic constants C_{11}, C_{12}, and C_{44}, two of which (C_{11} and C_{12}) can be calculated from the bulk modulus and the tetragonal shear constant C'. Moreover, the equilibrium volume (lattice constant) is obtained by fitting the total energy-volume data with Murnaghan's equation of state [34]. The bulk modulus (B) for a cubic crystal is equal to $B = (C_{11} + 2C_{12})/3$ and can be obtained from the second derivative of the energy-volume curve. The remaining elastic constant C_{44} can be calculated by a monoclinic volume-conserving distortion [35,36]

$$\epsilon = \begin{bmatrix} 0 & \delta/2 & 0 \\ \delta/2 & 0 & 0 \\ 0 & 0 & \delta^2/(4-\delta^2) \end{bmatrix}, \tag{1}$$

where the energy is given by

$$E(\delta) = 1/2C_{44}\delta^2 + O(\delta^4). \tag{2}$$

The tetragonal shear constant C' is

$$C' = \frac{C_{11} - C_{12}}{2}, \tag{3}$$

TABLE I. Calculated zero-temperature values of the $B2$ phase for the equilibrium lattice parameters (a), elastic constants (C_{11}, C_{12}, C_{44}, and C'), bulk modulus (B), Zener anisotropy (A), and melting temperatures (T_m) of XZn (X = Cu, Ag, and Au) along with available experimental values.

Alloys	CuZn	AgZn	AuZn
a (Å)	2.970 (2.954)[a]	3.192 (3.159)[d]	3.195 (3.149)[e]
C_{11} (GPa)	126.3 (129.1)[b]	92.1 (101.9)[d]	121.3 (147.4)[e]
C_{12} (GPa)	110.5 (109.7)[b]	85.0	109.3 (133.9)[e]
C_{44} (GPa)	89.3 (82.4)[b]	52.5 (54.8)[d]	62.0 (62.26)[e]
C' (GPa)	7.9 (9.70)[b]	3.55	6.0 (6.72)[e]
B (GPa)	115.7 (116.2)[b]	87.3	113.3 (138.4)[e]
A	11.30 (8.50)[b]	14.80	10.33 (9.26)[e]
T_m (K)	1299 ± 300 (1162)[c]	1097 ± 300 (944)[c]	1270 ± 300 (1058)[c]

[a]Reference [39].
[b]Reference [40].
[c]Reference [41].
[d]Graphical extrapolation of data in Ref. [14].
[e]Reference [42].

and the strain matrix is given by

$$\epsilon = \begin{bmatrix} \delta & 0 & 0 \\ 0 & -\delta & 0 \\ 0 & 0 & \delta^2/(1-\delta^2) \end{bmatrix}. \quad (4)$$

The equation for the energy with the distortion can be written as

$$E(\delta) = 2C'\delta^2 + O(\delta^4). \quad (5)$$

The bulk modulus is calculated from the volume-pressure relation

$$B(V) = -V\frac{\partial P}{\partial V} = \frac{\partial^2 E(V)}{\partial V^2}. \quad (6)$$

The calculated elastic constants can be used to estimate the melting temperature of cubic metals and compounds through the empirical (linear) relationship between C_{11} and the melting temperature of cubic solids [37], given by

$$T_m = 553 + \frac{5.91\ \text{K}}{\text{GPa}} C_{11} \pm 300\ \text{K}. \quad (7)$$

The typical error bar of this relationship (±300 K) is also indicated in the table.

III. STABILITY OF $B2$ CRYSTAL STRUCTURE

The $B2$ phase is a CsCl type structure with $Pm\bar{3}m$ group symmetry. The ground-state properties and elastic parameters for the $B2$ phases of XZn (X = Cu, Ag, and Au) have been calculated and are presented in Table I. The theoretical results are generally in good agreement with the available experimental data. The calculated melting temperatures seem consistently high by a couple of hundred degrees but track the experimental trend relative to the Cu, Ag, and Au compounds.

The Zener anisotropy factor A is defined as the ratio of the C_{44} and C' elastic constants. According to Zener [38], the elastic anisotropy of the lattice and the tendency for a material to display a structural phase transformation are interrelated. He proposed that there is a mechanical instability in the bcc phase caused by a high elastic anisotropy. More specifically, it was found that a bcc phase with small elastic constant C' (weak shear resistance) promotes elastic anisotropy, while alloys for which $A > 6$ are unstable and often display a structural (martensitic) phase transformation [38].

The calculated anisotropy factors A for CuZn, AgZn, and AuZn are nonmonotonic, 11.3, 14.8, and 10.4, respectively. As these values are much greater than 6, according to Zener the $B2$ phase of these alloys should not be stable and should have a tendency towards a structural phase transformation [10,16,43].

AgZn, which has the highest anisotropy factor among these alloys, also has the smallest elastic parameters and hence suggests that the $B2$ phase for this system is highly unstable relative to the other systems [10]. In fact, this phase can only form during a quench from the disordered bcc phase [11,13]. In order to understand the importance of chemical bonds and atomic-size effects on stability or instability of XZn systems, we calculated their chemical and elastic formation energies.

IV. CHEMICAL AND ELASTIC FORMATION ENERGIES

The separation of the formation energy of alloys into the chemical and elastic formation energies directly shows the competition between the strength of the X-Zn interatomic bonding and the size effect (strain) between constituent atoms. The chemical formation energy ΔH_{chem} of a binary alloy is the difference between the total energy of the compound in equilibrium, $E(A_xB_{1-x})$, and the component energies, $E(A_x)$ and $E(B_{1-x})$ (cf. Refs. [44–46]). The chemical formation energy of a binary compound with concentration x is thus given by

$$\Delta H_{\text{chem}} = E(A_xB_{1-x};(\bar{a})) - xE_A(\bar{a}) - (1-x)E_B(\bar{a}). \quad (8)$$

The elastic formation energy ΔH_{elast} is the necessary energy needed to distort pure components A and B from their respective equilibrium lattice constants a_A^0 and a_B^0, to the lattice constant $\bar{a}$ of the combined system, and is given by [44–46]

$$\Delta H_{\text{elast}} = \left[E_A(\bar{a}) - E_A\left(a_A^0\right)\right] + (1-x)\left[E_B(\bar{a}) - E_B\left(a_B^0\right)\right]. \quad (9)$$

Although the zero-temperature crystal structures of X and Zn atoms are different from bcc (viz., face-centered cubic or fcc for the noble metals and hexagonal close-packed or hcp for Zn), in order to minimize the effect of directional bonding between atoms, we used the bcc phase as the reference state for all of the elements studied here. To better understand effects of the atomic size on the stability of the XZn systems, the chemical and elastic energies of AgZn and AuZn were calculated at both their calculated equilibrium volumes (lattice constants) as well as at the CuZn equilibrium volume (i.e.,

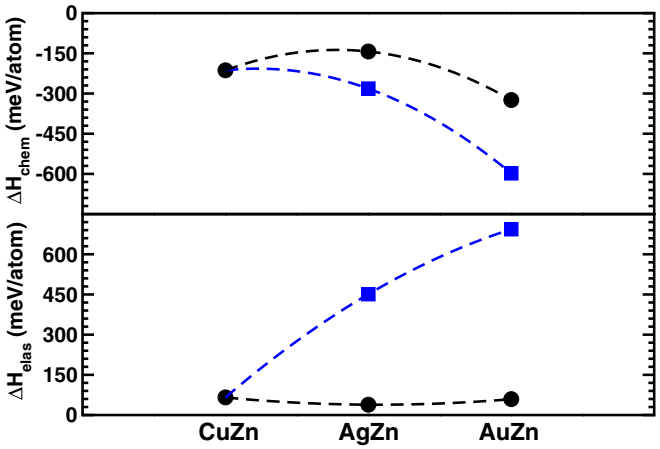

FIG. 1. Calculated chemical and elastic formation energies for the XZn (X = Cu, Ag, Au) $B2$ phase. The solid circles are the calculated energies at the equilibrium volume of each system, while the solid squares are the energies of AgZn and AuZn at the CuZn equilibrium volume. The dashed lines are guides for the eye.

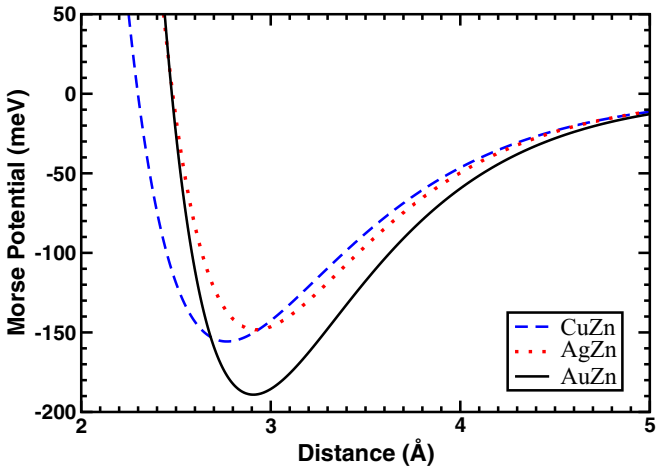

FIG. 2. Morse potential model for XZn (X = Cu, Ag, Au) bonds in the $B2$ phase which is fitted up to the fourth-nearest neighbors.

using the same fixed CuZn lattice constants for the formation energy calculations for all three compounds).

Calculated chemical and elastic formation energies for different alloys are depicted in Fig. 1. As shown, if all three compounds used the same fixed CuZn equilibrium lattice constant, the chemical energy of the systems follow a monotonic trend. That is, CuZn has the highest chemical energy and AuZn the lowest while the energy of AgZn will be in between. This chemical energy trend shows that the increased spatial extent of the d orbital systematically increases the Cu-Zn bond strength, when the distance between the X and Zn atoms is fixed. However, this causes the elastic energies of AgZn and AuZn to become very large due to the increasing atom size of Cu, Ag, and Zn (which manifests as a larger and larger core-core repulsion term when modeled with pair potentials; see below). The result is to expand the lattice constants when the AgZn and AuZn equilibrium volumes are calculated. This reduces the elastic energies of all three systems at their equilibrium volumes, which have comparably small values. The competition between these two opposing formation-energy trends gives rise to the maximum in the chemical formation energy for AgZn in the curve calculated for equilibrium volumes of each compound (solid circles in Fig. 1). We next examine this effect in a more detailed manner by using a pair-potential model to estimate the interaction between the neighboring atoms.

V. PAIR-POTENTIAL MODEL

The Morse potential has been widely used to model and estimate chemical bonds or the bond strength between atoms in solids [47,48] and in diatomic molecules [25]. This potential has competing attractive and repulsive terms that give rise to a minimum separation between the atoms that corresponds to their equilibrium distance. The potential is given by

$$\Phi(r_{ij}) = D[e^{-2\alpha(r_{ij}-r_0)} - 2e^{-\alpha(r_{ij}-r_0)}], \qquad (10)$$

where $\Phi(r_{ij})$ is the potential energy (interaction) between two atoms separated by a distance r_{ij}, D and α are potential parameters, and r_0 is the distance where the potential is a minimum.

When we use a Morse potential, we ignore any explicit directional dependence of the bonding (no dependence on bond angles is included in the parameters). This is suitable for our situation since all of the structures of interest have $B2$ symmetry, viz., the bcc and $B2$ crystal structures. The high symmetry of the cubic structures should minimize any directional bonding effects, and enables us to focus on the magnitude of the relative bond strength, which is the main quantity of interest for us. For other less symmetric crystal structures, it may be important to include directional effects in the modeling.

Our fits for the Morse potential were extended up to fourth-nearest-shell interactions with improved agreement when including more shells of interactions [49]. The first-principles calculations of the total energy for different volumes of the pure elements were used to determine the bcc X-X and Zn-Zn potential parameters. Then, these same calculated X-X and Zn-Zn parameters were used in the energy versus volume curves of the XZn alloys to obtain the X-Zn potential parameters. A similar approach has been successfully used for modeling the interactions in Ni-Al systems [50].

The calculated Morse potentials for different X-Zn atoms are shown in Fig. 2. The relative bond-strength trend is in complete agreement with the predicted chemical-energy formation of the system (Fig. 1). Since our analysis shows that the nearest-neighbor interactions are the major contribution to the XZn phase stability, this indicates Ag-Zn is the weakest bond in XZn (X = Cu, Ag, Au). What essentially is happening is that the X-Zn bond becomes stronger and stronger for fixed atom distance as one goes down the column of the periodic table, since $5d$ orbitals are more extended than $4d$ orbitals which are more extended than $3d$ orbitals, increasing hybridization with the Zn orbitals. However, opposing this effect is an increased X-Zn atomic distance from the lattice expansion caused by the core-core repulsion (of the larger atomic cores as one goes down the column), which reduces the

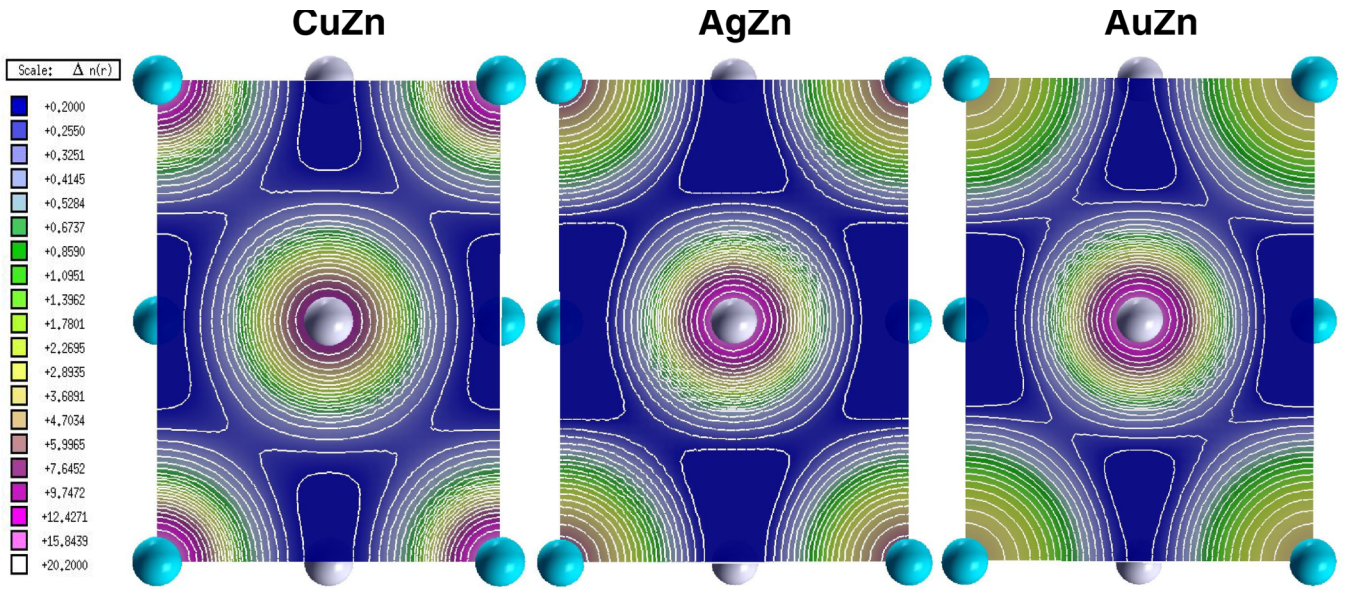

FIG. 3. The charge-density distribution of *X*Zn alloys in the [110] plane where the Zn atom is at the center and the *X* atoms are at the corners.

overlap of these wave functions. Initially, the distance effect dominates and the AgZn bond is weaker than the CuZn bond, but then the increased *d*-wave orbital spatial extent of Au wins out, and the AuZn bond becomes strongest of all. The dominance of this effect is that the lattice constant is almost identical between AgZn and AuZn. The larger Au core wants to push the atoms farther apart, but is not able to accomplish this due to the increased AuZn bond strength. This result can also explain the small elastic parameters of the AgZn system relative to the CuZn and AuZn alloys.

VI. CHARGE-DENSITY DISTRIBUTION AND DENSITY OF STATES

The charge-density distribution for the *B*2 *X*Zn phases in the [110] plane is depicted in Fig. 3 for each system. In each figure, the atoms in the center represent Zn, with *X* (either Cu, Ag, or Au) shown at the corners [51]. A closer examination of the contour map of the electron charge density plot suggests that the electron charge density between Ag and Zn is the lowest of all the *X*Zn alloys, in agreement with the chemical potential formation energies and the Morse potential fits.

To better understand the nature of the bonding between the atoms in different systems the electronic partial densities of states have been calculated and analyzed. Figures 4, 5, and 6 and Table II show the Zn *s* and *p* and *X d* symmetry decompositions and their integrated values of the densities of states for the *B*2 CuZn, AgZn, and AuZn alloys.

To study the role of size effects on the stability of the structures, the AgZn and AuZn partial densities of states (PDOSs) are calculated at the CuZn lattice constant ($a = 2.970$ Å) as well as at their relaxed or equilibrium lattice constants ($a = 3.192$ and 3.195 Å, respectively). As shown in Fig. 4, the Cu *d* band in CuZn is more localized (narrower, with sharper features) than for the Ag and Au *d* bands. However, the Zn *s-p* bands in CuZn are broader than is the case for AgZn and AuZn, indicating better bonding between Cu *d* and Zn *s-p* bands. The hybridization between the Zn *s-p* bands and the Cu *d* band has also been verified independently with the KKR-CPA method [52]. In AgZn (Fig. 5), the Ag *d* band and Zn *s-p* bands at the CuZn lattice constant are wider than at its equilibrium lattice constant, as an expected band narrowing for expanded lattice constants (larger distance between the atoms and hence reduced hybridizations). The broader bands indicate better hybridization between the Ag and Zn atoms in agreement with the chemical formation energy trends (Fig. 1). However, due to the much bigger atomic radius of Ag with respect to Cu, the AgZn alloy has a very high strain energy, resulting in an expanded equilibrium lattice constant for AgZn relative to that of CuZn. As a consequence, the hybridization between Ag and Zn drops significantly (narrower bands) resulting in a weaker bonding between Ag and Zn atoms (Fig. 5).

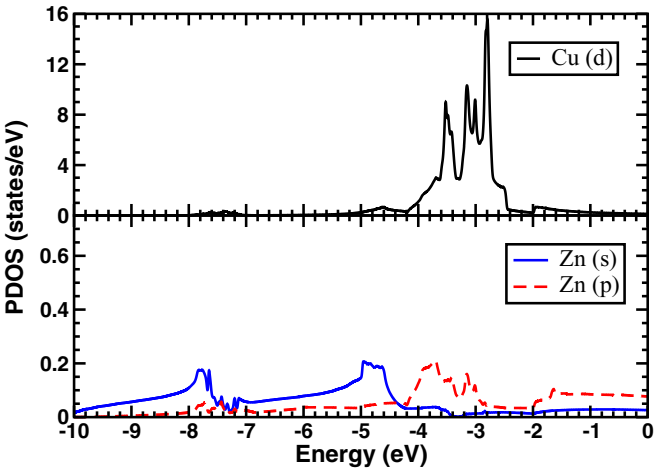

FIG. 4. Partial densities of states (Fermi level at 0) for the Cu *d* states (upper panel) and for the Zn *s* and *p* states (lower panel).

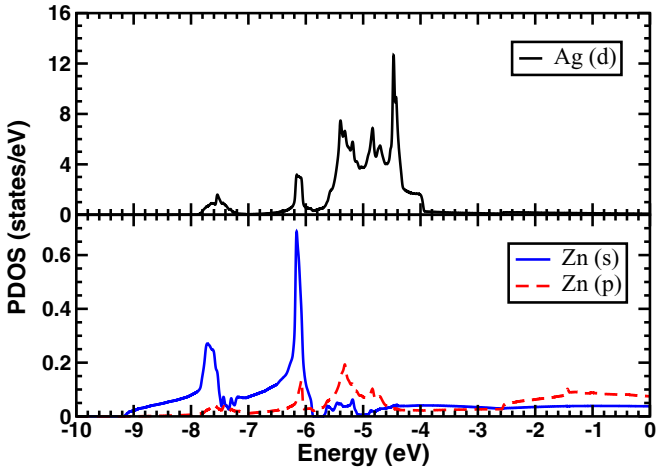

FIG. 5. A comparison of the partial densities of states (Fermi level at 0) for the Ag d states (upper panel) and for the Zn s and p states (lower panel), both at the AgZn relaxed (equilibrium) lattice constant of 3.192 Å and at that for CuZn, 2.970 Å.

AuZn is similar to AgZn, with stronger Au-Zn bonds at smaller lattice constants (Fig. 6). However, despite this, Fig. 6 shows that the relaxed Au $5d$ orbital is still more extended than for Cu or Ag, causing the strongest bonding among all of these compounds.

In order to estimate the order and relative size of the bond energies in these alloys for the d orbitals of Cu, Ag, and Au atoms, this was calculated at different lattice constants using the equation

$$E_{\text{bond}} = \int^{E_f} (E - E_c) n(E) dE. \tag{11}$$

In this equation, $n(E)$ is the density of states, E_f the Fermi energy, and E_c the energy of the center of the band. For the case of the d band, E_c is the energy when the orbital is half filled (5 electrons). The results of the bond energies

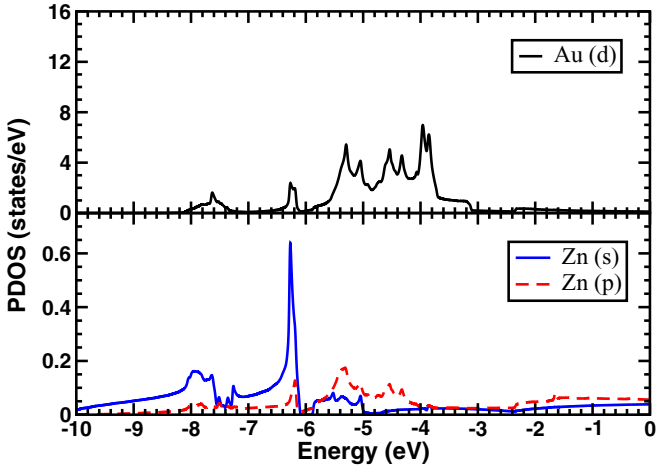

FIG. 6. A comparison of the partial densities of states (Fermi level at 0) for the Au d states (upper panel) and for the Zn s and p states (lower panel), both at the AuZn relaxed (equilibrium) lattice constant of 3.195 Å and at that for CuZn, 2.970 Å.

TABLE II. Integrated number of electrons for Zn s and p and X d symmetry decompositions.

Alloy	Zn (s)	Zn (p)	X (d)
CuZn	0.573	0.521	9.174
AgZn	0.588	0.582	8.899
AgZn (relaxed)	0.552	0.404	8.900
AuZn	0.565	0.615	8.731
AuZn (relaxed)	0.514	0.414	8.676

are depicted in Fig. 7. As discussed in the introduction, in the XZn system, when all three calculations are done at the same CuZn lattice constant, the d-bond energy of the X atoms decrease monotonically (Fig. 7). However, at their relaxed or equilibrium lattice constants the bond energies are nonmonotonic, with the Ag d bond having the highest energy, and Au the lowest. This shows the role played by repulsive atomic cores in changing the lattice constant, which in turn modifies the relative d-bond energies.

Based on the chemical-strain formation energies, pair-potential modeling, charge-density distributions, band-structure analysis, and d-bond energies, one can explain the nature of the weak bonding between Ag-Zn atoms as a consequence of the competition between the effect of the d-orbital spatial extent on the X-Zn hybridizations and the atomic-size effect (core-core repulsion expanding the lattices). In the next section, calculations are extended to finite temperature and it is shown that bond strength also influences the stability of the $B2$ structure at high temperatures.

VII. STABILITY OF $B2$ VERSUS $A2$ STRUCTURES AT FINITE TEMPERATURE

A. The heat of formation of ordered and disordered bcc phases

The heat of formation (or formation energy) is the amount of energy added or released when a compound is formed from the separate elements; it indicates whether it is favorable to create the material or not. It also is a measure of the relative

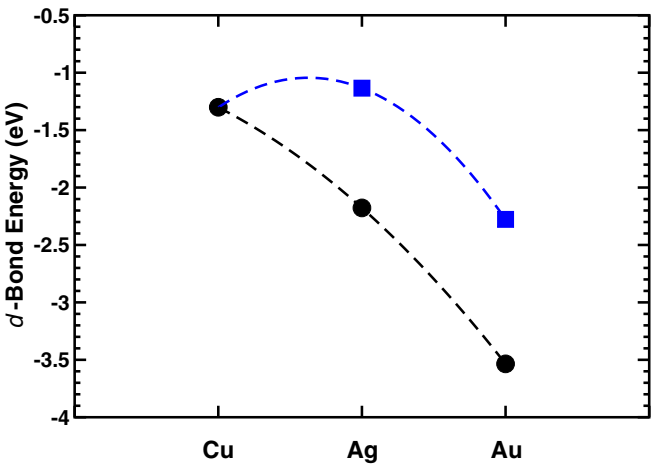

FIG. 7. d-bond energies of Cu, Ag, and Au at lattice constant of CuZn (solid circles) and their relaxed (equilibrium) lattice constants (solid squares). The dashed lines are guides for the eye.

TABLE III. Calculated values at 0 K of Cu, Ag, Au, Zn elements for equilibrium lattice parameter (a), c/a ratio, and bulk modulus (B), with some available experimental values.

Elements	Phase	a (Å)	c/a	B (GPa)
Cu	fcc	3.63 (3.61)[a]		136.18 (142.03)[b]
Ag	fcc	4.16 (4.09)[a]		88.84 (108.72)[c]
Au	fcc	4.17 (4.08)[a]		132.08 (180.32)[c]
Zn	hcp	2.66 (2.66)[a]	1.867 (1.856)[a]	79 (84.70)[d]

[a]Reference [39].
[b]Reference [54].
[c]Reference [55].
[d]Reference [56].

stability of the different compounds, providing an estimate of the effective bonding strength. The heat of formation, ΔH, of a binary alloy $A_{1-x}B_x$ can be calculated from

$$\Delta H(A_{1-x}B_x) = E(A_{1-x}B_x) - (1-x)E(A) - xE(B), \tag{12}$$

where $E(A_{1-x}B_x)$ is the total energy of the binary structure, and $E(A)$ and $E(B)$ are the energies of the elements with x mole concentration, each in its equilibrium state [53]. In this work, formation energies are calculated at zero kelvin, and free energy contributions to the formation energy are neglected.

To calculate the formation energies of the XZn compounds, the ground-state energies of the X and Zn elements are required. Cu, Ag, and Au have face-centered cubic (fcc) crystal structures at zero temperature and pressure, while Zn has a stable hexagonal close-packed (hcp) crystal structure. All calculations were performed on relaxed lattices at their equilibrium volumes and atomic positions, with all structural parameters chosen to minimize the total energy. The calculated ground-state properties, such as the equilibrium lattice constants a and the bulk moduli B, are given in Table III, where their values are compared to the corresponding available experimental data, indicating good agreement. It should be noted that including the spin-orbit interaction for Au increased the calculated bulk modulus by 20 GPa, in better agreement with experimental measurement.

To study the disordered bcc phases, in principle we should do ensemble averages of the energy of the system over many different disordered configurations. This would require a huge number of calculations and would be extremely difficult. To get around this, we employ a common trick in alloy calculations of replacing the ensemble average with a single approximate surrogate structure whose total energy is expected to be an excellent approximation to the average energy that would have been found by performing the ensemble average. For our surrogate structure we have used a particular special quasirandom structure (SQS; in our case, with a 32-atom periodic cell) to represent our effective disordered system [57]. The $B2$ and SQS heats of formation that we have calculated using this structure are summarized in Table IV and Fig. 8.

Three points are apparent when examining this data: First, the negative heat of formation demonstrates that the bcc ordered and disordered XZn structures are stable materials relative to their pure elements. In addition, it is shown that the $B2$ heat of formation is lower (more stable) than that of SQS for all three materials. Second, when comparing the relative energy differences between the $B2$ and SQS phases, that of AgZn is much smaller than CuZn or AuZn, and, in fact, AuZn has an especially large difference. Since the entropy at high temperatures tends to favor disorder, in the absence of any other information, these results immediately suggest that at lower temperatures there is likely to be ordered $B2$ phases for CuZn and AuZn, with the case of AgZn less clear. In fact, this is consistent with the experimental phase diagram. For example, the $B2$ AuZn structure is so stable that it is retained all the way to melting and the disordered bcc phase never forms at all (hence the energy phase stability difference is stronger than the entropy effects of configuration mixing). CuZn has a disordered phase at high temperature that then transforms to an ordered $B2$ phase at lower temperatures. AgZn is also disordered at high temperatures but can form the $B2$ phase only by quenching. The final and third point that can be surmised from the data is that the relative order of bonding strength is AuZn (highest), CuZn, and AgZn (lowest) in the disordered phase, just as we found previously in our calculations for the ordered $B2$ phase.

TABLE IV. Calculated values of the $B2$ and SQS phases for the heat of formation of XZn (X = Cu, Ag, and Au) alloys, calculated at 0 K.

Alloys	Phase	ΔH (meV/atom)
CuZn	$B2$	− 90.4
	SQS	− 50.8
AgZn	$B2$	− 47.9
	SQS	− 22.8
AuZn	$B2$	− 211.5
	SQS	− 146.0

B. The bcc order-disorder transition temperature

As expected and shown in previous studies [58], a good transition temperature for the order-disorder transformation

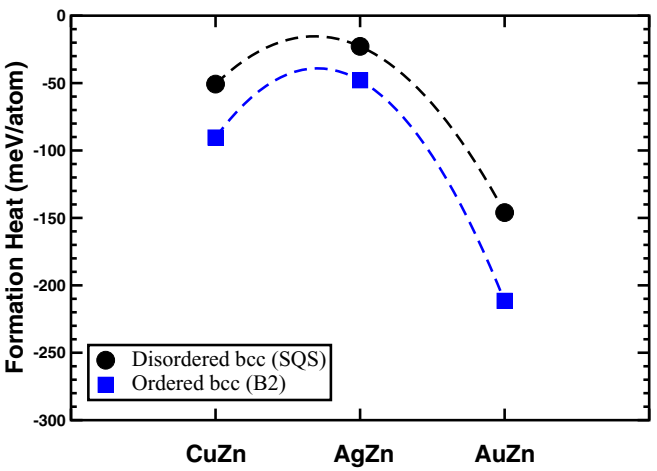

FIG. 8. Calculated heat of formation for the XZn $B2$ and SQS phases. The dashed lines are guides for the eye.

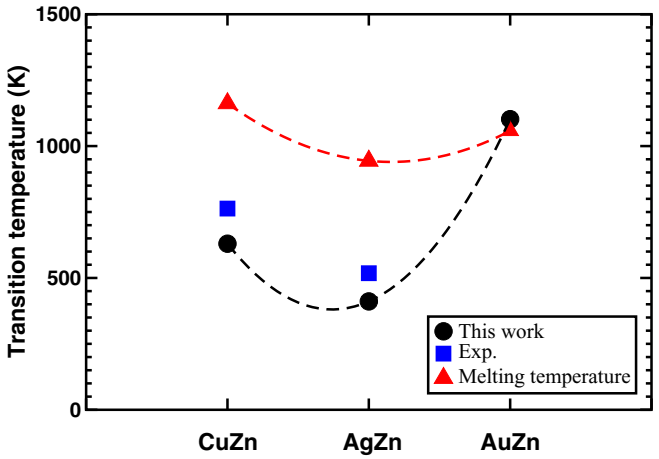

FIG. 9. Calculated order-disorder transition temperatures for *X*Zn and their comparison with experimental values [10] and melting temperatures [41]. The dashed lines are guides for the eye.

can be obtained by only including the configurational entropy contribution to the free energy. The configurational entropy of a binary alloy is given by [53]

$$S_{\text{ideal}} = -k_b[x \ln x + (1-x)\ln(1-x)], \tag{13}$$

where k_b is the Boltzmann constant and x is the concentration of the atom, and has a value of $S_{\text{ideal}} = -0.69k_b$ for 50% concentration. The order-disorder transition temperature can then be obtained from the following equation:

$$T \approx \frac{\Delta H_{SQS} - \Delta H_{XZn}}{S_{\text{ideal}}}. \tag{14}$$

The calculated transition temperatures and their measured values and the melting temperatures of each system are shown in Fig. 9.

For all the alloys, the predicted order-disorder transition temperatures are systematically about 100 K too low, which can be caused by either the neglect of contributions from the vibrational and electronic entropies, or also perhaps from systematic errors arising from the use of the SQS structure as a surrogate for the ensemble average of the disordered system. However, the predicted transition temperatures follow the same trend seen in the experiments (which is a justification for our use of the SQS structure); they also follow a similar pattern to that observed in the *differences* in the heat of formation between the ordered and disordered structures ($B2$ and SQS) shown in Fig. 8. This is reasonable because these differences indicate how much energy it takes to disorder the material. As mentioned above, these differences in turn appear to track the relative value of the magnitude of the heats of formation for the ordered structures, suggesting that the effective bond strength is actually the ultimate controlling factor setting the energy (or temperature) scale for all of these processes.

More specifically, with respect to Fig. 9, AuZn had the most stable $B2$ structure relative to SQS and has a theoretically predicted transition temperature slightly above melting, consistent with no order-disorder transition (experimentally, AuZn remains in the $B2$ structure all the way to melting [59]). CuZn has a larger difference than AgZn, which is consistent with the higher transition temperature for CuZn relative to AgZn (i.e., the more stable the $B2$ structure is relative to the disordered SQS, the higher the temperature it takes to provide enough entropy to disorder the material).

VIII. SUMMARY

In this study, first-principles calculations were performed to investigate the formation and stability of the ordered and disordered bcc phases in CuZn, AgZn, and AuZn alloys. We demonstrated that the nonmonotonic behavior of many of the properties of these materials, as one goes down the noble-metal column of the periodic table, results from a competition between atomic-core size and the spatial extent of the noble-metal d orbitals for different principal quantum numbers. The first effect pushes the atoms apart reducing hybridization, whereas the second increases hybridization, leading to a minimum in the X-Zn bonding strength for AgZn relative to CuZn and AuZn. These results were confirmed in detail by using pair-potential modeling, charge-density analysis, and studies of the partial density of states. It was specifically shown that the Ag-Zn bond is indeed the weakest of the *X*Zn systems, while the AuZn is the strongest. The weak Ag-Zn bond is responsible for the structural instability of the $B2$ phase and the lower order-disorder transition temperature. Moreover, the strong Au-Zn bond is responsible for the stability of the ordered phase all the way up to the melting temperature, unlike for CuZn and AgZn which disorder before melting.

Pair-potential modeling confirmed this result, which explains chemical and elastic formation energy trends in these materials. In addition, in agreement with experimental observations, calculations of the anisotropy factor of the *X*Zn systems confirm that the $B2$ AgZn alloy is structurally unstable relative to the other systems. Furthermore, while AgZn has the lowest critical temperature, the disordered bcc phase for AuZn does not exist.

The special quasirandom structure (SQS) was used to estimate the energy of the disordered bcc phase of the *X*Zn materials. Calculated formation energies of ordered and disordered bcc phases were used to estimate the bcc order-disorder transition temperature in all systems, which were found to be in good agreement with the experimental measurements. In addition, the AuZn order-disorder transition temperature is higher than its melting temperature, confirming that the disordered phase cannot form in this system.

ACKNOWLEDGMENTS

This work was carried out under the auspices of the National Nuclear Security Administration of the US Department of Energy at Los Alamos National Laboratory under Contract No. DE-AC52-06NA25396. We also acknowledge the generous amounts of computer time provided by Texas Tech University High Performance Computer Center. O.A. gratefully acknowledge the financial support from the Umm al-Qura University.

[1] A. Lavakumar, *Concepts in Physical Metallurgy* (Morgan & Claypool Publishers, San Rafael, 2017), Chap. 9.

[2] A. R. Jha, *Next-Generation Batteries and Fuel Cells for Commercial, Military, and Space Applications* (CRC, Boca Raton, 2012).

[3] S. Berchmans, A. J. Bandodkar, W. Jia, J. Rammirez, Y. S. Meng, and J. Wang, J. Mater. Chem. A **2**, 15788 (2014).

[4] J. C. Lashley, S. M. Shapiro, B. L. Winn, C. P. Opeil, M. E. Manley, A. Alatas, W. Ratcliff, T. Park, R. A. Fisher, B. Mihaila, P. Riseborough, E. K. H. Salje, and J. L. Smith, Phys. Rev. Lett. **101**, 135703 (2008).

[5] M. Sanati, R. C. Albers, T. Lookman, and A. Saxena, Phys. Rev. B **88**, 024110 (2013).

[6] T. B. Massalski and H. W. King, Prog. Mater. Sci. **10**, 3 (1963).

[7] W. Hume-Rothery, R. W. Smallman, and C. W. Haworth, *The Structure of Metals and Alloys* (Institute of Metals, London, 1969).

[8] P. E. A. Turchi, M. Sluiter, F. J. Pinski, D. D. Johnson, D. M. Nicholson, G. M. Stocks, and J. B. Staunton, Phys. Rev. Lett. **67**, 1779 (1991).

[9] H. Warlimont, *Physical Properties of Martensite and Bainite* (Iron and Steel Ins., 1965), Special Rep. 93, p. 58.

[10] Y. Murakami and S. Kachi, Jpn. J. Appl. Phys. **13**, 1728 (1974).

[11] W. Kitchingman and J. Buckley, Acta Metall. **8**, 373 (1960).

[12] S. Noguchi, J. Phys. Soc. Jpn. **17**, 1844 (1962).

[13] D. Arias and J. E. Kittl, Metallography **11**, 429 (1978).

[14] Y. Matsuo, T. Suzuki, and A. Nagasawa, J. Phys. Soc. Jpn. **49**, 1344 (1980).

[15] R. Orr and J. Rovel, Acta Metall. **10**, 935 (1962).

[16] H. Pops and T. Massalski, Trans. AIME **233**, 728 (1965).

[17] H. Pops and T. Massalski, Acta Metall. **15**, 1770 (1967).

[18] J. Abriata, O. Bressan, C. Luengo, and D. Thoulouze, Phys. Rev. B **2**, 1464 (1970).

[19] G. Blair and D. Downie, Met. Sci. J. **4**, 1 (1970).

[20] H. Iwasaki, T. Fujimura, M. Ichikawa, S. Endo, and M. Wakatsuki, J. Phys. Chem. Solids **46**, 463 (1985).

[21] Y. Matsuo, K. Ohshima, H. Iwasaki, Y. Kuroiwa, H. Maeta, and K. Haruna, J. Phys. F **18**, 2505 (1988).

[22] T. B. Massalski, H. Okamoto, P. Subramanian, and L. Kacprzak (eds.), *Binary Alloy Phase Diagrams*, 2nd ed. (ASM International, Materials Park, 1990), Vol. 1, p. 117 and 456, Vol. 2, p. 1508.

[23] B. Magyari-Köpe, G. Grimvall, and L. Vitos, Phys. Rev. B **66**, 064210 (2002).

[24] T. W. Darling, F. Chu, A. Migliori, D. J. Thoma, M. Lopez, J. C. Lashley, B. E. Lang, J. Boerio-Goates, and B. F. Woodfield, Philos. Mag. B **82**, 825 (2002).

[25] P. M. Morse, Phys. Rev. **34**, 57 (1929).

[26] VASP 2003 at http://www.vasp.at.

[27] G. Kresse and J. Hafner, Phys. Rev. B **47**, 558 (1993).

[28] G. Kresse and J. Furthmuller, Phys. Rev. B **54**, 11169 (1996).

[29] J. P. Perdew, K. Burke, and M. Ernzerhof, Phys. Rev. Lett. **77**, 3865 (1996).

[30] P. E. Blöchl, Phys. Rev. B **50**, 17953 (1994).

[31] G. Kresse and D. Joubert, Phys. Rev. B **59**, 1758 (1999).

[32] G. Kresse and J. Furthmuller, Comput. Mater. Sci. **6**, 15 (1996).

[33] P. E. Blöchl, O. Jepsen, and O. K. Andersen, Phys. Rev. B **49**, 16223 (1994).

[34] F. D. Murnaghan, Proc. Natl. Acad. Sci. USA **30**, 244 (1944).

[35] M. Mehl, J. Osburn, D. Papaconstantopoulos, and B. Klein, Phys. Rev. B **41**, 10311 (1990).

[36] L. Vitos, *Computational Quantum Mechanics for Materials Engineers: The EMTO Method and Applications* (Springer-Verlag, London, 2007).

[37] M. Fine, L. Brown, and H. Marcus, Scr. Metall. **18**, 951 (1984).

[38] C. Zener, Phys. Rev. **71**, 846 (1947).

[39] W. B. Pearson, *A Handbook of Lattice Spacings and Structures of Metals and Alloys* (Pergamon, Oxford, 1964), Vol. 2.

[40] D. Lazarus, Phys. Rev. **76**, 545 (1949).

[41] H. Baker (ed.), *ASM Handbook, Vol. 3, Alloy Phase Diagrams* (ASM International, Materials Park, 1992).

[42] R. Schiltz Jr., T. Prevender, and J. Smith, J. Appl. Phys. **42**, 4680 (1971).

[43] G. Grimvall, B. Magyari-Kope, V. Ozolins, and K. Persson, Rev. Mod. Phys. **84**, 945 (2012).

[44] L. G. Wang and A. Zunger, Phys. Rev. B **67**, 092103 (2003).

[45] Z. W. Lu, S.-H. Wei, and A. Zunger, Phys. Rev. Lett. **66**, 1753 (1991).

[46] Z. W. Lu, S.-H. Wei, and A. Zunger, Europhys. Lett. **21**, 221 (1993).

[47] L. A. Girifalco and V. G. Weizer, Phys. Rev. **114**, 687 (1959).

[48] R. Lincoln, K. Koliwad, and P. Ghate, Phys. Rev. **157**, 463 (1967).

[49] H. Ipser, J. P. Neumann, and Y. Austin Chang, Monatshefte für Chemie **107**, 1471 (1976).

[50] M. Sanati, R. C. Albers, and F. Pinski, J. Phys.: Condens. Matter **13**, 5387 (2001).

[51] A. Kokalj, Comput. Mater. Sci. **28**, 155 (2003).

[52] W. M. Temmerman, P. J. Durham, Z. Szotek, M. Sob, and C. G. Larsson, J. Phys. F **18**, 2387 (1988).

[53] R. E. Watson and M. Weinert, in *Solid State Physics*, edited by H. Ehrenreich and F. Spaepen (Academic Press, San Diego, 2001), Vol. 56, p. 87.

[54] W. C. Overton Jr. and J. Gaffney, Phys. Rev. **98**, 969 (1955).

[55] J. R. Neighbours and G. A. Alers, Phys. Rev. **111**, 707 (1958).

[56] G. A. Alers and J. R. Neighbours, J. Phys. Chem. Solids **7**, 58 (1958).

[57] G. Ghosh, A. van de Walle, and M. Asta, Acta Mater. **56**, 3202 (2008).

[58] C. Jiang, C. Wolverton, J. Sofo, L.-Q. Chen, and Z.-K. Liu, Phys. Rev. B **69**, 214202 (2004).

[59] E. Owen and I. Edmunds, Proc. Phys. Soc. **50**, 389 (1938).